AIP | Journal of Applied Physics

TaN interface properties and electric field cycling effects on ferroelectric Si-doped HfO2 thin films

Patrick D. Lomenzo, Qanit Takmeel, Chuanzhen Zhou, Chris M. Fancher, Eric Lambers, Nicholas G. Rudawski, Jacob L. Jones, Saeed Moghaddam, and Toshikazu Nishida

Citation: Journal of Applied Physics **117**, 134105 (2015); doi: 10.1063/1.4916715
View online: http://dx.doi.org/10.1063/1.4916715
View Table of Contents: http://scitation.aip.org/content/aip/journal/jap/117/13?ver=pdfcov
Published by the AIP Publishing

TaN interface properties and electric field cycling effects on ferroelectric Si-doped HfO_2 thin films

Patrick D. Lomenzo,[1] Qanit Takmeel,[2] Chuanzhen Zhou,[3] Chris M. Fancher,[4] Eric Lambers,[5] Nicholas G. Rudawski,[5] Jacob L. Jones,[4] Saeed Moghaddam,[6] and Toshikazu Nishida[1,a)]

[1]*Department of Electrical and Computer Engineering, University of Florida, Gainesville, Florida 32611, USA*
[2]*Department of Materials Science and Engineering at the University of Florida, Gainesville, Florida 32611, USA*
[3]*Analytical Instrumentation Center, College of Engineering at North Carolina State University, Raleigh, North Carolina 27696, USA*
[4]*Department of Materials Science and Engineering at North Carolina State University, Raleigh, North Carolina 27696, USA*
[5]*Major Analytical Instrumentation Center at the University of Florida, Gainesville, Florida 32611, USA*
[6]*Department of Mechanical and Aerospace Engineering at the University of Florida, Gainesville, Florida 32611, USA*

(Received 3 December 2014; accepted 22 March 2015; published online 6 April 2015)

Ferroelectric HfO_2-based thin films, which can exhibit ferroelectric properties down to sub-10 nm thicknesses, are a promising candidate for emerging high density memory technologies. As the ferroelectric thickness continues to shrink, the electrode-ferroelectric interface properties play an increasingly important role. We investigate the TaN interface properties on 10 nm thick Si-doped HfO_2 thin films fabricated in a TaN metal-ferroelectric-metal stack which exhibit highly asymmetric ferroelectric characteristics. To understand the asymmetric behavior of the ferroelectric characteristics of the Si-doped HfO_2 thin films, the chemical interface properties of sputtered TaN bottom and top electrodes are probed with x-ray photoelectron spectroscopy. Ta-O bonds at the bottom electrode interface and a significant presence of Hf-N bonds at both electrode interfaces are identified. It is shown that the chemical heterogeneity of the bottom and top electrode interfaces gives rise to an internal electric field, which causes the as-grown ferroelectric domains to preferentially polarize to screen positively charged oxygen vacancies aggregated at the oxidized bottom electrode interface. Electric field cycling is shown to reduce the internal electric field with a concomitant increase in remanent polarization and decrease in relative permittivity. Through an analysis of pulsed transient switching currents, back-switching is observed in Si-doped HfO_2 thin films with pinched hysteresis loops and is shown to be influenced by the internal electric field. © *2015 AIP Publishing LLC*. [http://dx.doi.org/10.1063/1.4916715]

I. INTRODUCTION

Growing reports on HfO_2-based ferroelectric thin films[1–8] are striking renewed interest in ferroelectrics for memory applications[9–11] and energy storage.[12] Si-doped HfO_2 thin films were the first ferroelectric HfO_2-based thin films reported with Böscke *et al.* showing that the crystallization of the Si:HfO_2 thin films in the presence of a capping TiN electrode can lead to the emergence of ferroelectric and antiferroelectric properties.[1] Robust retention characteristics of Si-doped HfO_2 ferroelectrics are promising for ferroelectric random access memory (FRAM) applications.[13] Further investigations into ferroelectric Si-doped HfO_2 thin films have illustrated the wide variety of process conditions which can influence the ferroelectric and electrical properties of Si-doped HfO_2 such as the choice of capping electrode,[14] the influence of the HfO_2 film thickness,[15] and the effects of Si-dopant layering.[16] In addition, the recent observation of ferroelectric domains through piezoresponse force microscopy in Si-doped HfO_2 thin films distinguishes its behavior from electrets and electrochemical responses.[17]

Due to the very small thicknesses (sub-10 nm) in which ferroelectricity can be achieved in Si-doped HfO_2, the role of the electrodes and the electrode-ferroelectric interfaces on the ferroelectric behavior in the thin films cannot be overstated. Si-doped HfO_2 thin films with TiN electrodes have been shown to exhibit the so-called "wake-up" effect in which the remanent polarization increases and the internal electric field decreases with electric field cycling.[18] Zhou *et al.*[18] ascribed this effect to the difference in charge carrier concentrations between the bottom and top TiN electrodes whereby the removal or redistribution of mobile charge during bipolar cycling was believed to subsequently decrease the internal electric field and de-pin ferroelectric domains, although direct evidence of the chemical nature of the bottom and top TiN electrodes was not presented. The stability of the two ferroelectric polarization states, a prerequisite for nonvolatile memory applications, deteriorates with the existence of an internal or depolarization electric field. We use the term depolarizing field to signify the specific case when an internal electric field destabilizes a given polarization state. The term internal electric field (or internal bias) is employed more generally to describe the shifted ferroelectric characteristics along the electric field axis, often referred to

a)Electronic mail: nishida@ufl.edu

as imprint, which stabilizes one polarization state at the expense of the other. Since doped ferroelectric HfO_2 thin films are being pursued to increase the memory density of FRAM[19] and to establish the scalability of ferroelectric field effect transistors (FeFETs),[11] the presence of a depolarizing field is highly undesirable. In addition, antiferroelectric-like characteristics observed in HfO_2-based films could be related to internal bias fields,[20] but no direct evidence has been established yet. Understanding the origin of the internal electric field and the effects of electric field cycling in doped ferroelectric HfO_2 thin films thus remains an important task from a scientific and technological perspective.

It is known that large surface electric fields originating from the spontaneous polarization of ferroelectrics cause band bending and ionization of trap states at the ferroelectric-electrode interface.[21–23] Brennan[21] points out several important factors which influence the space charge distribution and the depolarization field in ferroelectric thin films. First, ionization of trap states at the ferroelectric-electrode interface will continue to increase until the surface space charge can effectively screen the internal polarization of the ferroelectric; it is through the unequal distribution of space charge between the top and bottom electrode (BE) interfaces which then gives rise to a depolarizing field. Second, the metal electrodes form Schottky contacts which provide a sheet of electrons at the electrode interface to maintain charge neutrality with the positive space charge region established on the ferroelectric side of the junction. Lastly, the space charge profile at the ferroelectric/electrode interfaces is influenced by the ferroelectric polarization, Schottky potential, and the applied electric field.

From the above arguments, it is clear that any investigation into the origin of an internal electric field observed in ferroelectric thin films should begin at the electrode/ferroelectric interfaces. To this end, we use x-ray photoelectron spectroscopy (XPS) to characterize the chemical properties of the top and bottom electrode interfaces of TaN metal-ferroelectric-metal (MFM) capacitors which exhibit a large internal bias. The as-grown ferroelectric domains present in the film are shown to be oriented upward away from the bottom TaN electrode. Electric field cycling reduces the internal bias, increases the remanent polarization (P_r), and decreases the relative permittivity, but is not sufficient to obtain symmetric ferroelectric properties. Since this "wake-up" effect has been proposed to originate from the asymmetry in the bottom and top electrodes (TEs)[18] and such a large internal bias has not been seen in HfO_2-based devices with symmetric electrode materials, direct evidence of the chemical behavior of the electrode interfaces between TaN and Si-doped HfO_2 provides timely insight into the growing body of knowledge for thin film HfO_2-based ferroelectrics.

II. EXPERIMENTAL

TaN BEs approximately 8.5 nm thick were RF sputtered on a highly doped (0.001–0.005 Ω cm) (100) p-Si substrate, which had undergone a buffered oxide etch (BOE, 6:1, 40% NH_4F:49% HF in H_2O). The BOE was used to etch the native SiO_2 layer from the Si-substrate to reduce the bottom contact resistance before the TaN BE deposition. After TaN BE deposition, a 10 nm thick HfO_2:SiO_2 layered film was grown using plasma enhanced atomic layer deposition (PEALD) with a substrate temperature of 200 °C. Tetrakis(dimethylamino)hafnium and Tris(dimethylamino)silane were used as the HfO_2 and SiO_2 precursors, respectively. Time of flight-secondary ion mass spectrometry (TOF-SIMS) and XPS were used to determine the Si mol. % of the HfO_2 thin films corresponding to 24:1 and 16:1 ALD cycling ratios of HfO_2 and SiO_2. The Si content was determined to be 1.2 and 1.6 Si mol. %, respectively. XPS and TOF-SIMS were found to be within 0.1 mol. % agreement. TOF-SIMS quantification of Si was achieved using standards which were created through ion implantation of Si into HfO_2. TOF-SIMS analyses were conducted using a TOF-SIMS V instrument equipped with a Bi_n^{m+} (n = 1–5, $m = 1, 2$) liquid metal ion gun. Approximately 8.5 nm thick TaN TEs were RF sputtered on the Si-doped HfO_2 thin films. Unless specified otherwise, the 1.2 and 1.6 mol. % Si-doped HfO_2 thin films were annealed at 700 °C and 800 °C for 20 s respectively in nitrogen to crystallize the Si-doped HfO_2 thin films. 100 nm thick Ir contacts were then sputtered and subsequently lifted off to serve as a hard mask. Wet etching was carried out with a 6:1.1:1 (H_2O:H_2O_2:NH_4OH) SC1 solution at 65 °C, a similar recipe has been reported to yield greater than 100:1 selectivity between TaN:HfO_2.[24] The patterned capacitors are 10000 μm^2.

We note that in our previous work,[14,16] the Si concentration was measured in metal/HfO_2:Si/SiO_2/Si capacitors where we witnessed Si diffusion into the HfO_2 film from the substrate, which led to a larger incorporated Si concentration. Furthermore, the lack of a clear boundary between the likely formation of a hafnium silicate layer at the HfO_2/SiO_2 interface in metal/HfO_2:Si/SiO_2/Si structures, the inhomogeneous nature of the Si-doping profile, and the weak sensitivity factor of Si relative to Hf and O in XPS make quantification of small concentrations of Si in thin film HfO_2 nontrivial. Hence, we believe it is helpful to provide the ALD cycling ratio which was used to fabricate the HfO_2:Si thin films since the ferroelectric characteristics can also be tuned through the Si-dopant layering profile.[16] It should be pointed out that Mueller *et al.*[25] used a 16:1 HfO_2:SiO_2 ALD cycling ratio which achieved 3.8 mol. % Si where we only observe 1.6 mol. % Si in our films; however, variations in the actual Si concentration for a given ALD cycle ratio can be expected due to different deposition tools, deposition temperatures, and oxidizers to name just a few factors.

Hysteresis measurements were carried out on the MFM capacitors with a Sawyer-Tower circuit at 1 kHz to obtain the polarization–electric field (P–E) plots. An Agilent 4294A was used to take capacitance-voltage (C-V) measurements with an AC signal amplitude of 50 mV at 50 kHz to extract the relative permittivity characteristics of the Si-doped HfO_2 thin films. Voltage cycling was performed with bipolar square waves at 1 kHz and the terms "unpoled" and "pulse poled" will be used to describe ferroelectric films before and after cycling respectively. Unless specified otherwise, all bipolar cycling was performed with an electric field magnitude of 3.5 MV/cm. Pulsed transient current measurements were carried out with an Agilent 33511B waveform

generator with a 50 Ω resistor in series with the ferroelectric capacitor. Electrical pulses during the extracted switching current transients had a 100 ms delay time. All electrical measurements were performed with the bottom electrode grounded.

XPS was carried out through a Phi 5000 Versaprobe II with a monochromated Al-Kα source (1486.6 eV), an exit angle of 45°, a pass energy of 23.5 eV, and the spectrum was aligned by putting the C1s binding energy at 284.8 eV. The XPS analysis beam spot size was 200 μm in diameter. *In situ* depth profiling during XPS was achieved using an Ar^+ gun with an accelerating voltage ranging from 0.5 keV to 3.0 keV. Grazing incidence X-ray diffraction (GIXRD) patterns were measured using a Rigaku Smartlab diffractometer with a 0.5° angle of incidence. GIXRD patterns were measured from 10° to 95° 2θ with a step size of 0.05° and a 2 s/step counting time. High-resolution cross-sectional transmission electron microscopy (HR-XTEM) was used to investigate the structure of the capacitors and measure the thicknesses of the different layers using a JEOL 2010F transmission electron microscope operated at 200 kV and equipped with a Gatan Orius SC200B digital camera. HR-XTEM specimens were prepared using an FEI DB235 scanning electron microscope/Ga^+ focused ion beam system using methods described elsewhere;[26–29] care was taken to minimize sidewall damage to the specimens by performing the final milling steps using a 5 kV Ga^+ beam.[30,31] The specimens were prepared such that the thin dimension (foil normal) corresponded to an in-plane ⟨110⟩ direction; during HR-XTEM imaging, the specimen was oriented such that the incident beam was aligned to this direction.

III. RESULTS AND DISCUSSION

The hysteresis loop of the Si-doped HfO_2 thin films with TaN electrodes is shifted in the positive direction along the electric field axis as can be seen in Fig. 1. The coercive field, E_c, Eq. (1) is usually determined by the electric field values for which the polarization becomes zero in the P-E curve.

$$E_c = \frac{|E_c^+| + |E_c^-|}{2}. \tag{1}$$

For as-fabricated devices, a coercive field of 0.85 MV/cm was extracted from the P-E curve, while an approximately 1.2 MV/cm coercive field was obtained for both Si-doped HfO_2 thin films after electric field cycling. The cycled film's coercive field is higher than the coercive field value of ~1 MV/cm first reported for Si-doped HfO_2 ferroelectric thin films with TiN electrodes.[1] Alternatively, the coercive field can be determined by the peaks in the switching current, which in our case results in a larger coercive field of 1.4 MV/cm for the pulse poled ferroelectric films. Since the switching current peaks in the unpoled ferroelectric capacitors have coercive values of 1.3 MV/cm and are in much closer agreement with the pulse poled device, the current transient method yields a more consistent determination of the coercive field value which is not expected to change in magnitude with electric field cycling. Schenk *et al.* have provided a review on the usefulness of the transient current analysis during hysteresis measurements.[20] The negative coercive field in the as-fabricated ferroelectric capacitors is ~0 MV/cm as seen clearly in the negative switching current peaks in Figs. 1(a) and 1(c). An internal electric field, E_I, Eq. (2) is produced from the significant asymmetry in the negative and positive coercive fields.

$$E_I = \frac{|E_c^+| - |E_c^-|}{2}. \tag{2}$$

The unpoled Si-doped HfO_2 thin films with TaN electrodes exhibit a 1.3 MV/cm internal electric field. Furthermore,

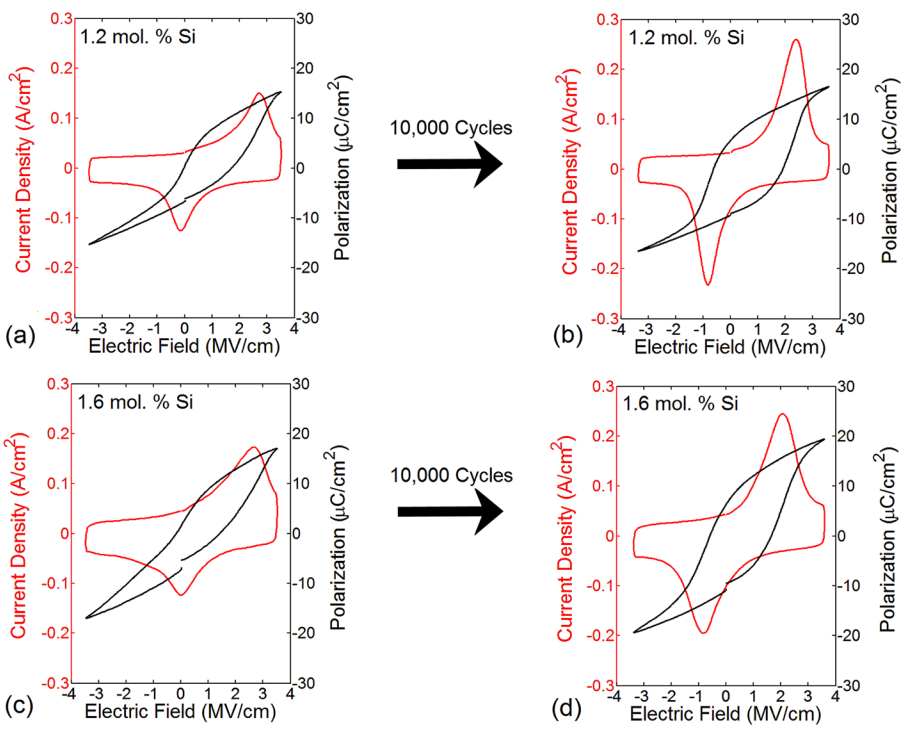

FIG. 1. Hysteresis of the 1.2 mol. % Si films before (a) and after (b) 10 000 bipolar cycles illustrates the large increase in P_r and reduction of the internal bias. The 1.6 mol. % Si doped-HfO_2 thin films exhibit the same characteristics before (c) and after (d) cycling, but has a slightly larger background leakage current relative to the current switching peaks due to the higher anneal temperature. Both as-fabricated films have a negative coercive field ~0 MV/cm and a positive remanent polarization of ~0 $\mu C/cm^2$, indicating that the as-grown ferroelectric domains are pointing upward away from the TaN bottom electrode.

the positive P_r value is $\sim 0\ \mu C/cm^2$ which indicates that the as-grown ferroelectric domains are aligned in one direction pointing toward the top electrode. The situation can be illustrated by looking more closely at the current transients in Figs. 1(a) and 1(c). As the ferroelectric is being excited by the clockwise triangle wave during hysteresis, the switching current peak occurs at about 2.6 MV/cm during the ramp upward. However, on the return to 0 MV/cm, the ferroelectric Si-doped HfO_2 thin films already begins switching back to its original state. Hence, there is only one stable polarization state in the as-fabricated ferroelectric Si-doped HfO_2 thin films because of the overwhelming depolarization field domains encounter when they point downward toward the bottom electrode. Electric field cycling reduces the internal electric field to ~0.6 MV/cm in the Si-doped HfO_2 thin films after 10 000 bipolar cycles and increases both positive and negative remanent polarization values.

Similar to the observations made by Zhou *et al.*,[18] we observe a logarithmic increase in the remanent polarization during electric field cycling, Figs. 2(a) and 2(b), given by

$$P_r = P_{r0} + A \log(N), \tag{3}$$

where P_{r0} is the initial remanent polarization, A is the acceleration factor, and N is the number of bipolar cycles. The acceleration factor is larger for the positive remanent polarization and increases for stronger applied electric fields. The negative acceleration factor remains constant regardless of the magnitude of the electric field. The acceleration factors

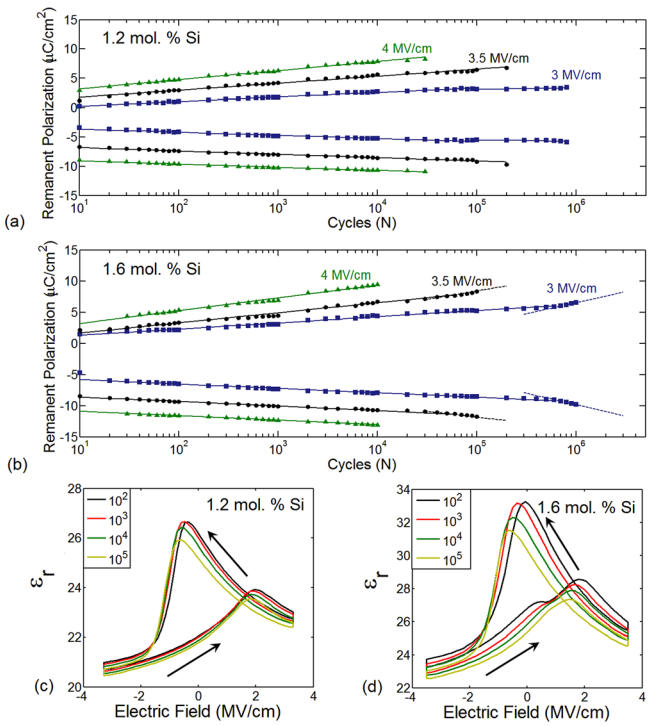

FIG. 2. The change in the remanent polarization for the (a) 1.2 mol. % Si-doped and the (b) 1.6 mol. % Si-doped HfO_2 thin films exhibits a logarithmic dependence with electric field cycling, experimental data are given by the symbols and the logarithmic fits are given by the solid line. A change in the slope before breakdown indicated an increase in the leakage current contribution toward P_r and is given by a dashed line. Changes in ε_r for both Si compositions (c) and (d) show the switching peaks shifting left and an overall decrease in relative permittivity with electric field cycling.

TABLE I. Acceleration factors obtained from the solid line logarithmic fits from Fig. 2.

	1.2 mol. % Si		1.6 mol. % Si	
Electric field (MV/cm)	A^+ ($\mu C/cm^2$)	A^- ($\mu C/cm^2$)	A^+ ($\mu C/cm^2$)	A^- ($\mu C/cm^2$)
3	0.334	−0.234	0.431	−0.309
3.5	0.521	−0.251	0.712	−0.317
4	0.676	−0.236	0.890	−0.310

extracted from the logarithmic fits are given in Table I. The simultaneous decrease in the internal electric field and increase in remanent polarization lend support to the hypothesis that the redistribution or compensation of electrically charged defects is occurring with bipolar cycling. Moreover, the strong dependency of the positive acceleration factor on the magnitude of the electric field suggests that the redistribution of charged defects or defect dipoles is occurring more strongly at one electrode interface in the ferroelectric Si-doped HfO_2 thin film with electric field cycling.

To gain more insight into the influence of electric field cycling and the underlying physical mechanisms behind the changes in the ferroelectric characteristics, C-V sweeps were performed to extract the changes in relative permittivity, ε_r, of the films. As can be seen in Figs. 2(c) and 2(d), the internal electric field causes highly asymmetric switching peaks. Similar ε_r characteristics have been observed in Si-doped HfO_2 with TiN electrodes[32] and 400 nm thick $Pb(Zr_{0.7}Ti_{.30})O_3$ with Pt electrodes.[33] The second ε_r peak in the forward sweep of the 1.6 mol. % Si doped HfO_2 thin film disappears with electric field cycling and will be discussed in more detail later. We observe that electric field cycling causes two significant changes in both of the Si-doped HfO_2 thin films. First, both switching peaks in the relative permittivity sweep shift leftward which adds further evidence that the internal electric field decreases with pulsed poling. Second, ε_r decreases with electric field cycling. Pulsed poling of $Pb(Zr_{.15}Ti_{.85})O_3$ has been shown to lead to 90° domain depinning through the reorientation or redistribution of charged defects or defect dipoles, which promoted an increase in P_r and a decrease in ε_r.[34] For the case of the lead zirconate titanate (PZT) material system, the increase in P_r and decrease in ε_r with electric field cycling are both associated with the conversion of tetragonal a-domains to c-domains.[34] Since the decrease in ε_r with electric field cycling of the ferroelectric Si-doped HfO_2 films is attended by an increase in remanent polarization, a similar phenomenon to 90° domain switching seen in PZT may be occurring. In particular, the higher ε_r tetragonal phase may become distorted with electric field cycling through the subsequent redistribution of charged defects or defect dipoles. Such a distortion of the tetragonal $P4_2/nmc$ phase may then lead to a transition to the lower ε_r noncentrosymmetric $Pca2_1$ or $Pmn2_1$ orthorhombic phases, which has been predicted by theoretical calculations.[35]

The crystal structure of the Si-doped HfO_2 thin films is consistent with the tetragonal or $Pca2_1$ orthorhombic phase[35] as confirmed by GIXRD (Fig. 3). The polar orthorhombic $Pca2_1$ space group was originally invoked to explain the

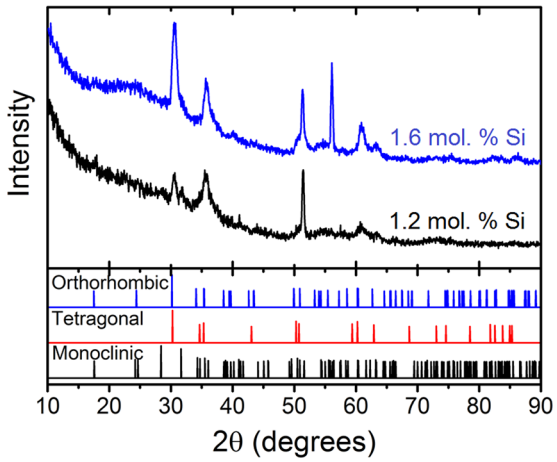

FIG. 3. GIXRD of the Si-doped HfO_2 thin films shows the crystal structure to be consistent with the tetragonal or orthorhombic phase for both compositions.

emergence of ferroelectric behavior in Si-doped HfO_2 thin films.[1] Theoretical work has shown that two polar orthorhombic space groups, $Pca2_1$ and $Pmn2_1$, have very close free energies and can be formed through a distortion of the nonpolar tetragonal $P4_2/nmc$ phase along the [001] and [100] directions respectively.[35] The concurrent increase in P_r and decrease in ε_r during electric field cycling are supportable by such a phase transformation, whereas the growth of an interfacial layer during pulsed poling would fail to explain the increase in P_r.

Up to this point, the asymmetry in the ferroelectric characteristics still remains unexplained. As was noted in the Introduction, the existence of an internal electric field is due to the unequal space charge densities at the top and bottom electrode/ferroelectric interfaces. Motivated by this understanding, XPS was used to evaluate the chemical behavior of the TaN TE and BE interfaces on the Si-doped HfO_2 thin films. Due to the very high selectivity (100:1) of the SC1 wet chemistry with respect to TaN and HfO_2,[24] the wet-etched surface provides an excellent snapshot of the TaN/HfO_2 TE interface composition. Henceforth, the SC1 wet etched surface will be referred to as the TE interface. Interestingly, a significant presence of Hf-N bonds is present at the TE interface as seen by the low energy shoulder in the Hf 4*f* binding energy, Fig. 4(a). A low intensity tantalum and nitrogen signal was also picked up at the TE interface during XPS. High resolution XPS scans show that the residual tantalum on the surface is primarily metallic (Ta^0) with only a small fraction of Ta-N bonds contributing to the Ta 4*f* binding energy at the TE interface, Fig. 4(b). Both Ta 4*f* and Hf 4*f* consist of a 4*f* 7/2 and 4*f* 5/2 spin doublet, which gives rise to two peaks for each chemical species. The N 1*s* binding energy shows contributions from both N-Hf and N-Ta bonds, Fig. 4(c). There are more N-Hf bonds than N-Ta bonds on the wet-

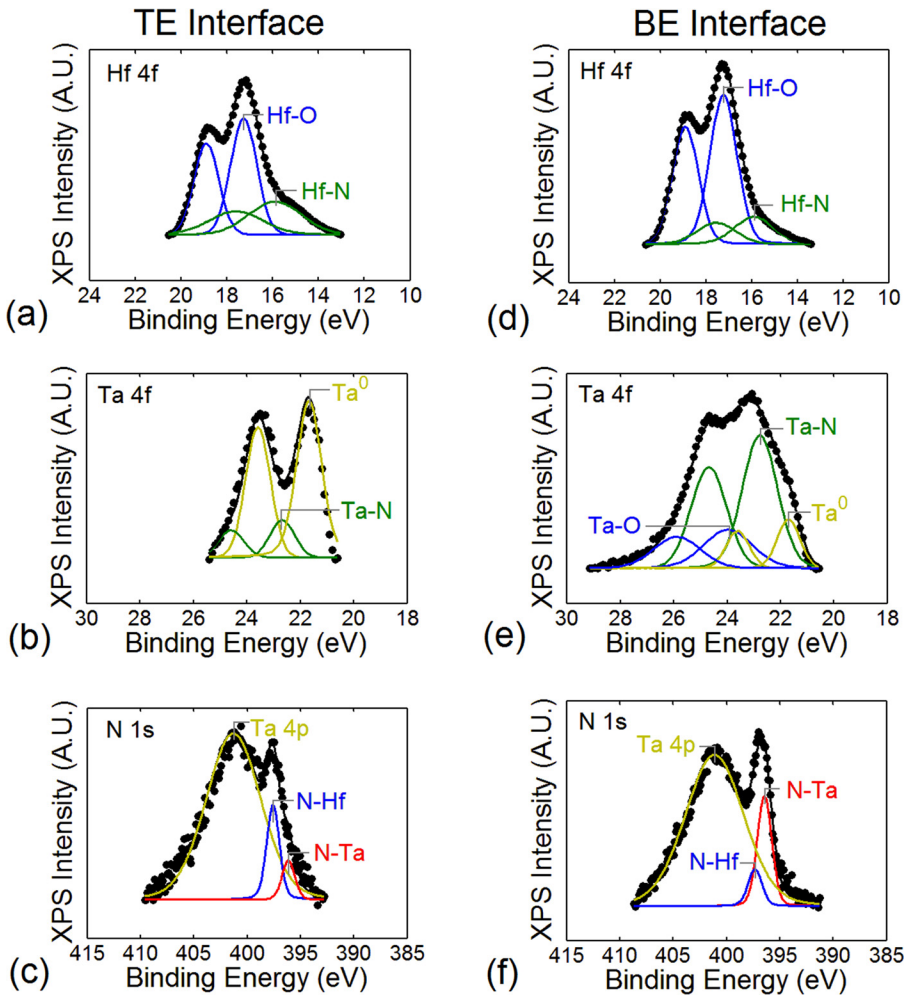

FIG. 4. XPS analysis of the TE interface shows (a) Hf-N bonds in Hf 4*f*, (b) residual metallic Ta^0 in Ta 4*f*, and (c) both N-Hf and Ta-N bonds in N 1*s*. The BE interface shows (d) Hf-N bonds in Hf 4*f*, (e) Ta-O bonds in Ta 4*f*, and (f) N-Hf and and N-Ta bonds in the N 1s binding energy.

etched TE interface, as seen by the greater contribution of N-Hf to the N 1*s* binding energy. The atomic concentration of tantalum at the TE interface is less than 4%, its detected presence after the SC1 wet etch is likely due to diffusion during the RTA and decomposition of interfacial TaN into Ta^0 and HfN. It should be noted that metallic Ta^0 has a lower etch rate than TaN for the SC1 chemistry, and since both Ta and TaN SC1 etch rates are larger than HfO_2, the TaN/HfO_2 interfacial surface composition is preserved without any contribution from the bulk of the TaN top electrode.

Using an Ar^+ ion beam during XPS, the Si-doped HfO_2 thin films were etched down to the BE interface to determine the chemical heterogeneity of the BE and TE interfaces. The Hf 4*f* binding energy at the BE interface confirms that Hf-N bonds are again present, Fig. 4(d). Significantly, the Ta 4*f* binding energy at the bottom electrode interface shows the presence of Ta-O bonds, Fig. 4(e), thus verifying that the bottom electrode TaN interface is oxidized. The exact oxidation state of Ta cannot be resolved, but TOF-SIMS yielded the most ionized molecular fragments for TaO_2 and Ta_2O_5 respectively. The presence of metallic Ta^0 and Hf-N bonds suggests decomposition of TaN at the BE interface during ALD or the rapid thermal anneal. The N 1*s* binding energy of the BE interface shows a greater degree of N-Ta bonds than N-Hf bonds, Fig. 4(f).

The observed N-Hf bonds at both electrode interfaces, in which the nitrogen atom substitutes for oxygen in the lattice, will effectively neutralize the gap states caused by oxygen vacancies and raise the valence band maximum by 0.2 eV.[36,37] Umezawa *et al.* found that when two nitrogen atoms occupy the nearest neighbor oxygen sites next to a neutral oxygen vacancy (V_O), each nitrogen atom extracts an electron and produces a positively charged oxygen vacancy (V_O^{2+}).[36] The addition of an electron to the two neighboring nitrogen atoms and the resulting production of a positively charged oxygen vacancy thus form an electric dipole.[36] Since both electrode interfaces contain substitutional nitrogen atoms at concentrations greater than 10 at. %, positively charged oxygen vacancies and the resulting N-V_O^{2+}-N dipole complexes are expected to be present in the films. Moreover, the redistribution of the positively charged oxygen vacancies and subsequent reorientation or randomization of the N-V_O^{2+}-N dipole complexes can explain the electric field cycling behavior in the Si-doped HfO_2 thin films. Since the bottom TaN interface is oxidized, the aggregation of V_O^{2+} at the BE interface will not be adequately screened by the sheet of electrons in the metal due to the physical separation interposed by the Ta_xO_y layer.

The situation can be visualized in Fig. 5. The internal bias present in the Si-doped HfO_2 thin films is caused by the accumulation of positively charged oxygen vacancies at the BE. Since the positively charged oxygen vacancies are not adequately screened at the oxidized TaN BE interface, the as-grown ferroelectric domains are polarized upward toward the TE. Thus, it is through the redistribution of V_O^{2+} accumulated at the BE interface which causes a decrease in the internal bias with electric field cycling. Oxidation of the bottom TiN electrode in ferroelectric $Hf_{0.5}Zr_{0.5}O_2$ films was also associated with a positive bias shift[38] and can be explained by this model. Further confirmation of the oxidation of the TaN/HfO_2 BE interface can be seen in Fig. 6. TEM shows a 1–2 nm thick Ta_xO_y layer present at the bottom electrode interface. The large 1.3–1.4 MV/cm coercive field observed earlier can be explained by the voltage drop across the Ta_xO_y layer, which will increase the measured value of E_c. Oxidation of the TaN BE interface occurred after exposure to air during the wafer transfer to the ALD chamber and subsequent exposure to oxygen plasma during the deposition of the Si:HfO_2 thin films. Since ferroelectric HfO_2-based thin films exhibit coercive fields 1–2 orders of magnitude larger than conventional perovskite ferroelectrics, shifts in the P-E loop are necessarily accompanied by larger space charge densities. Modeling the C-V characteristics after Brennan,[21] we extracted ionized charge densities on the order of 10^{19}–$10^{20}\,cm^{-3}$, which is 1–2 orders of magnitude larger than values extracted from lead zirconate titanate thin films[21,22] and supports the magnitude of the electric field shift observed in the hysteresis loop. It was found that in Sr-doped HfO_2 thin films, the activation energy for "wake-up" cycling and subsequent fatigue was found to be one order of magnitude lower than perovskites.[39] Schenk *et al.* suggested that the redistribution of oxygen vacancies and defects along domain

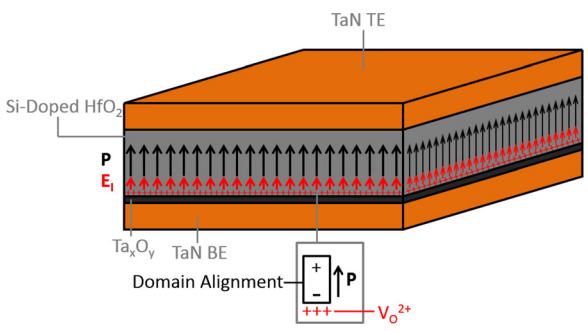

FIG. 5. As-grown ferroelectric domains are preferentially polarized upward toward the top electrode in the Si-doped HfO_2 thin films. The accumulation of positively charged oxygen vacancies at the oxidized TaN BE interface leads to the internal bias observed in the Si-doped HfO_2 thin films.

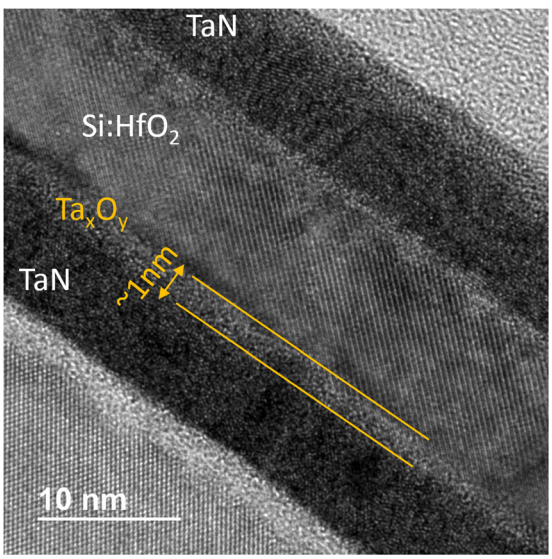

FIG. 6. TEM confirms the presence of a ~1 nm Ta_xO_y layer at the TaN BE interface.

or grain boundaries were likely candidates for "wake-up" and fatigue; the lower activation energies for these phenomena were attributed to the larger applied electric fields in HfO_2-based films compared to perovskite ferroelectrics.[39]

To determine if the switching kinetics were influenced by the internal electric field and the unequal space charge distribution, a variation of the Positive-Up-Negative-Down (PUND) pulse methodology[40] utilizing repeating Negative-Positive-Up (NPU) and Positive-Negative-Down (PND) pulse trains were used to calculate P_{sw}^{+} and P_{sw}^{-}, (4) as a function of pulse width.

$$\begin{cases} P_{sw}^{+} = \int J_{sw}^{+}(t)dt \\ P_{sw}^{-} = \int J_{sw}^{-}(t)dt \end{cases}. \tag{4}$$

The switching current densities are extracted from the PU and ND pulse sequences given by

$$\begin{cases} J_{sw}^{+}(t) = J_P(t) - J_U(t) \\ J_{sw}^{-}(t) = J_N(t) - J_D(t) \end{cases}. \tag{5}$$

Integrating the switching current density profile yields the switched charge resulting from the P and N pulses, while the transient polarization in the U and D terms is also taken into account. Since the dielectric response and leakage current are nominally the same in the PU and ND pulses, these contributions are effectively negated in Eq. (5). Thus, the pulsed transient current method has the advantage of being able to account for the leakage current, dielectric relaxation, and the charging/discharging currents so that a precise extraction of the polarization switching current can be made.

Similar to previous observations in ferroelectric Si-doped HfO_2 thin films,[25] we see a logarithmic dependence of switched charge with pulse width in cycled films (Fig. 7(a)), indicating that the thin films obey the nucleation limited switching model[41] whereby reverse nucleation of domains occurs through an ensemble of independently switching regions with a distribution of switching times. The as-fabricated films show power-law behavior with pulse-width and have steeper slopes than the poled devices. The power-law behavior can be attributed to the gradual redistribution of charged defects in the film during the measurement and is not believed to be an intrinsic property of the switching kinetics within the film. Electric field cycling produces a substantial increase in the switched polarization. The switching current density vs. electric field profiles for a 50 μs pulse width with a 1 μs rise time can be seen in Figs. 7(b)–7(e). Importantly, a small second switching current transient peak is observed in the as-fabricated 1.2 mol. % Si-doped HfO_2 thin film, Fig. 7(b), dashed line, indicating that an ensemble of domains have longer switching times when attempting to reverse nucleate against the internal electric field. This would suggest that the broad tail at the end of the positive switching current accounts for the switching of domains

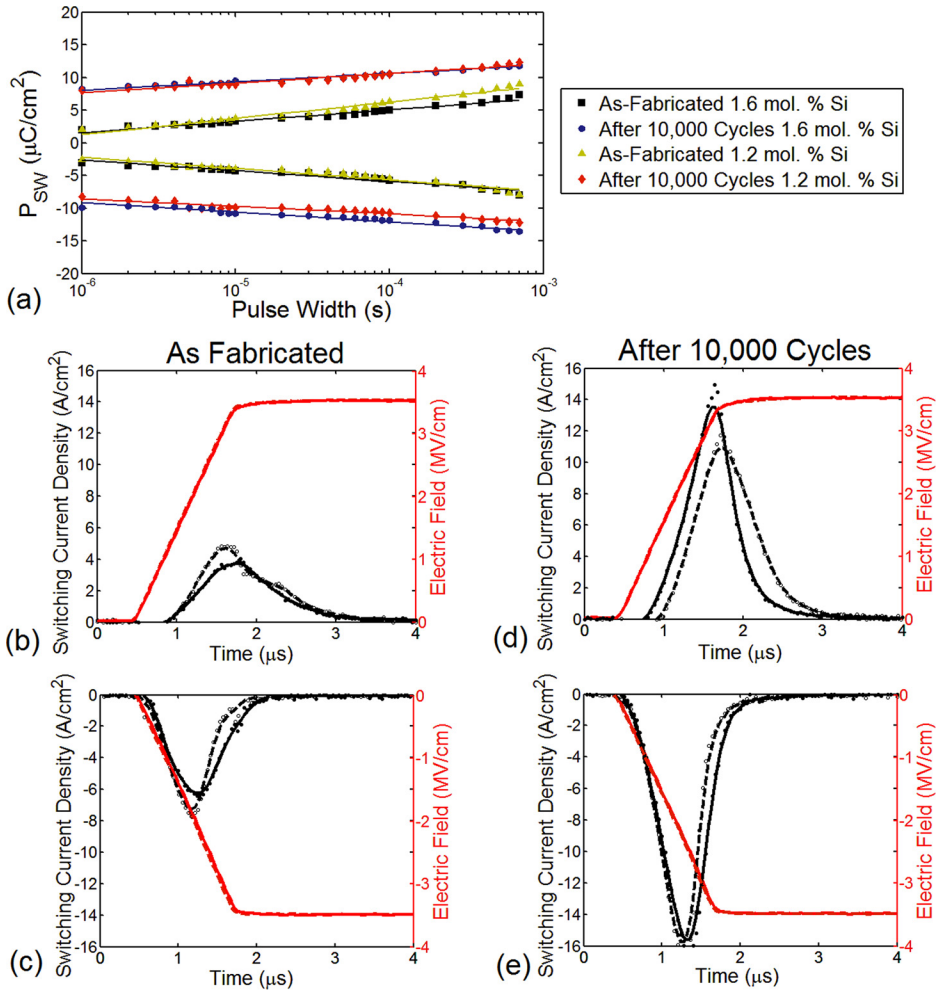

FIG. 7. (a) The switching kinetics of the Si-doped HfO_2 thin films follow a logarithmic dependence in accordance with the nucleation limited switching model, experimental data are given by the symbols and the logarithmic fits are given by the solid lines. (b)–(e) The switching current density before and after electric field cycling with the 1.2 mol. % and 1.6 mol. % Si-doped HfO_2 thin films are given by the dashed and solid lines, respectively, as discussed in the text. The pulse width is 50 μs with a 1 μs rise and fall time.

localized near the accumulation of positively charged oxygen vacancies and defect dipole complexes at the bottom TaN electrode. Switching occurs later when reverse nucleation must overcome the internal electric field, but cycling the capacitor decreases the mean switching time for domains nucleating under a positive electric field, while the switching time remains unchanged for applied negative electric fields before and after cycling. It can therefore be concluded that electric field cycling redistributes the defect charge or defect dipoles away from the TaN BE and permits faster reverse nucleation of domains at that interface.

Previous reports[1,15,17,42] on Si-doped HfO_2 thin films have shown antiferroelectric-like characteristics where the P-E loops were pinched. We observed pinched hysteresis loops in the Si-doped HfO_2 thin films which were doped with 1.6 mol. % Si and annealed at 700 °C for 20 s, Fig. 8(a). The current transient during hysteresis shows that the pinched P-E loop is accompanied by four broad and relatively low intensity current switching peaks in the four quadrants. This is expected for an antiferroelectric material[20] where two sub-lattices produce oppositely oriented polarization vectors and result in a net zero spontaneous polarization.[43] After electric field cycling, the hysteresis loop becomes narrow and de-pinched with only one clearly distinguishable switching peak because the merging of the negative current switching peaks cannot be resolved above the background leakage current, Fig. 8(b). The P-E loops in Fig. 8 are not symmetric because $P_r \approx P_r^-$ and $P_r^+ \approx 0\,\mu C/cm^2$, indicating that the defect charge at the bottom electrode is still influencing the antiferroelectric-like thin film's behavior. The ε_r vs. electric field profiles exhibit the double butterfly loop, which is well-known to occur in PZT-based antiferroelectrics.[44] Electric field cycling subsequently suppresses two out of the four ε_r peaks with an overall decrease in relative permittivity, Fig. 8(d). The resulting relative permittivity response to the electric field after cycling closely resembles the asymmetric switching peaks found in the ferroelectric Si:HfO_2 thin films in Fig. 2, corroborating evidence that defect charge is influencing the switching properties of the antiferroelectric-like film. Furthermore, the two permanent ε_r switching peaks shift leftward indicating a reduction in the internal electric field. As noted earlier, the decrease in relative permittivity and the reduction in the internal bias with electric field cycling could be due to a tetragonal → orthorhombic phase transition as a result of oxygen vacancy electromigration and reorientation or elimination of defect dipoles which stabilize the ferroelectric phase. Higher Si-doping concentrations can be used to stabilize antiferroelectric behavior in thin film Si:HfO_2 with little dependence on electric field cycling.[17]

To overcome the lack of detail in the current transient during hysteresis before and after electric field cycling, pulsed transient current analysis was used to obtain a closer look at the switching current density vs. electric field profile. As can be seen in Fig. 8(e), the as-fabricated films exhibit back-switching when a positive electric field is applied.

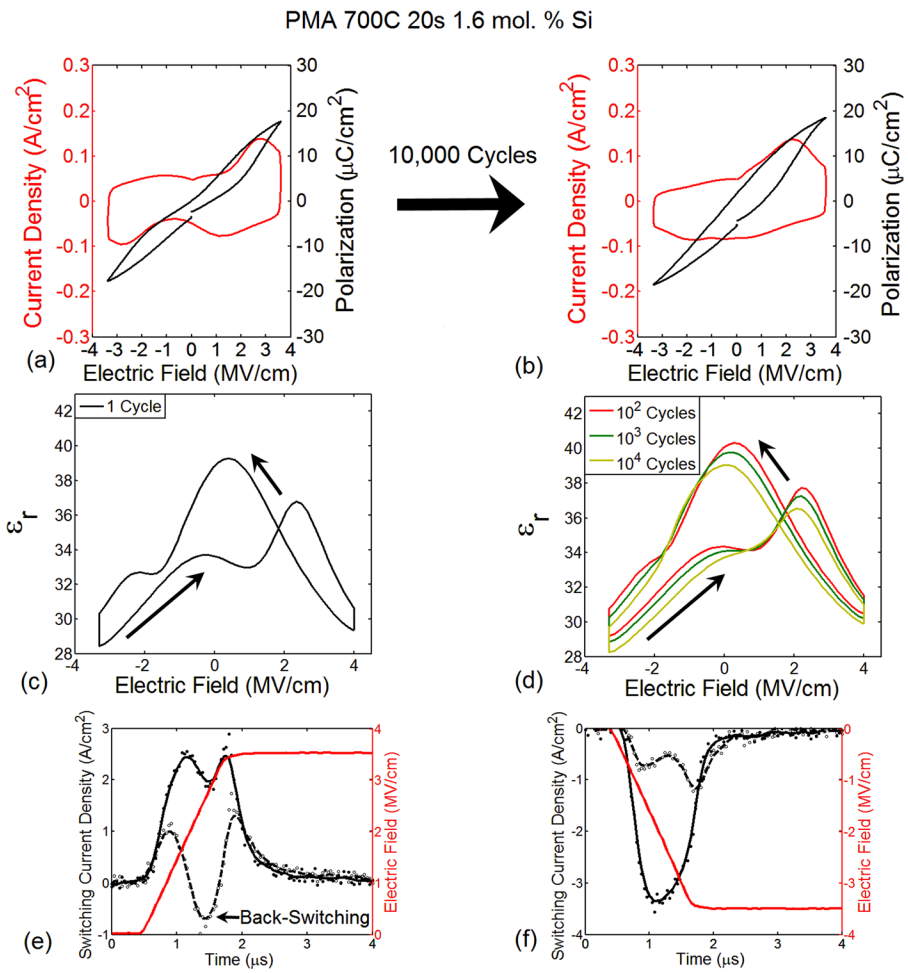

FIG. 8. With a lower temperature anneal, the 1.6 mol. % Si-doped HfO_2 thin films exhibit a pinched hysteresis loop (a) which opens up after electric field cycling (b). (c) Four ε_r peaks are observed as expected for an antiferroelectric material. (d) Cycling the Si:HfO_2 film results in the disappearance of two of the ε_r switching peaks. The switching current density vs. electric field profile shows (e) back-switching occurring for the as-fabricated films (dashed line) when nucleation must overcome the internal electric field. After 10 000 bipolar cycles (solid line), back-switching still occurs due to the depolarization field as seen by the minima in the switching current peak. (f) Switching currents in the direction of the internal electric field are still subject to back-switching (dashed line), but back-switching is suppressed after 10 000 bipolar cycles (solid line).

Back-switching is shown by the minima in the switching current profile and is due to the transient charge that is switched in the U pulse in the NPU pulse train. The inversion of the polarity of the switching current density in Fig. 8(e) possibly indicates a change in the switching kinetics of the transient polarization from the N → P and P → U pulse transitions. For this case, the switched charge in the U pulse exceeded the switched charge in the P pulse for a duration of time, although the total switched charged in the P pulse is larger overall indicating the presence of some ferroelectric domains within the antiferroelectric-like film. Back-switching current transients have also been observed in antiferroelectric $PbZrO_3$ thin films.[45] Cycling the film resulted in an overall increase in the forward switching current density and the magnitude of the back-switched charge was reduced. When negative electric fields are applied to the as-fabricated thin films, back-switching still occurs which is consistent for an antiferroelectric material since a ferroelectric → antiferroelectric transition will proceed when the applied electric field is removed. In this case, back-switching is found in the D pulse in the PND pulse train, where the transient polarization decay after the N pulse leads to domain switching in the D term. Cycling the film results in the merging of the two distinct negative switching current peaks and the switched charge increases in magnitude. Furthermore, back-switching is no longer appreciable in the pulsed current transient for negative electric fields after electric field cycling. Back-switching is exacerbated when domains have to reverse nucleate against the internal electric field as seen for applied positive electric fields in the antiferroelectric-like Si:HfO_2 thin films.

Overall, electric field cycling increases the switched charge in the antiferroelectric-like Si-doped HfO_2 films regardless of the polarity of the applied electric field and results in de-pinching of the hysteresis loop. The redistribution of positively charged oxygen vacancies and the reorientation or elimination of N-V_O^{2+}-N dipole complexes at the oxidized TaN BE is the most probable cause for the stabilization of the ferroelectric phase with electric field cycling in the pinched Si-doped HfO_2 thin films. We can conclude that the prevention of oxidation of the electrode interface, which can be achieved through *in situ* ALD deposition or careful selection of the electrode materials, is a prerequisite to avoid the development of internal electric fields in doped ferroelectric HfO_2 thin films.

IV. CONCLUSION

Ferroelectric Si-doped HfO_2 thin films with sputtered TaN electrodes were observed to have highly asymmetric ferroelectric characteristics due to the existence of a large internal electric field. Electric field cycling increased the remanent polarization and reduced the magnitude of the internal bias as a result of the redistribution of charged defects and defect dipoles. The chemical behavior of the TaN bottom and top electrode interfaces was analyzed using XPS and it was observed that both interfaces showed nitrogen incorporation into HfO_2, while only the bottom electrode interface was oxidized. It was deduced that the most likely candidate for the internal electric field was the aggregation of positively charged oxygen vacancies (V_O^{2+}) and N-V_O^{2+}-N dipoles at the oxidized BE interface. The physical separation between the accumulated positive charge at the BE interface was inadequately screened by the sheet of electrons in the TaN electrode because of the Ta_xO_y layer. The inadequate charge screening at the electrode interface caused the as-grown ferroelectric domains to preferentially polarize upward away from the bottom electrode.

The larger, field-dependent positive acceleration factor indicated that the redistribution of positively charged oxygen vacancies and the reorientation or elimination of defect dipole complexes at the BE occurred during electric field cycling. The simultaneous increase in P_r and decrease in relative permittivity were hypothesized to indicate structural changes in the Si-doped HfO_2 thin films as a result of the redistribution of the charged defects, notably a distortion of the higher ε_r tetragonal $P4_2/nmc$ phase to the lower ε_r $Pca2_1$ or $Pmn2_1$ polar orthorhombic phases. The switching kinetics showed the films to be governed by nucleation limited switching with longer nucleation times for domains reverse nucleating against the internal electric field. Electric field cycling improved the switching times and magnitude of the switched charge as a result of the redistribution of defect charge and defect dipoles at the BE interface. Si-doped HfO_2 thin films with pinched P-E loops exhibited four permittivity peaks and were observed to back-switch when having to reverse nucleate against the internal electric field. Subsequent cycling de-pinched the Si-doped HfO_2 thin films, reduced ε_r, caused the disappearance of two out of the four relative permittivity peaks, and increased the amount of switched charge due to the stabilization of the ferroelectric phase. The stabilization of the ferroelectric phase in ferroelectric capacitors with initially pinched P-E loops was concomitant with the reduction of the internal electric field due to the redistribution of charged defects and defect dipoles.

The emergence of internal electric fields arising from the unequal distribution of space charge at the electrodes can be detrimental to ferroelectric-based nonvolatile memory technologies because of the resulting instability of one of the polarization states. From this work, it can be concluded that *in situ* ALD electrode deposition may be beneficial to avoid oxidation of the electrode surface or that chemically inert electrode materials should be chosen to avoid the development of a depolarization field. This work established that the antiferroelectric-like characteristics of Si-doped HfO_2 can be influenced by an internal electric field, but the relationship between internal electric fields and antiferroelectric-like behavior in HfO_2-based films requires further investigation.

ACKNOWLEDGMENTS

The authors would like to acknowledge the use of the Nanoscale Research Facility and the Major Analytical Instrumentation Center at the University of Florida. The authors acknowledge the use of the Analytical Instrumentation Facility (AIF) at the North Carolina State University, which is supported by the State of North Carolina and the National Science Foundation. P.D.L. is a recipient of the Semiconductor Research Corporation Graduate Fellowship

award. T.N., J.L.J., and S.M. acknowledge support by the Semiconductor Research Corporation under 2013-RJ-2372G. J.J. and C.Z. acknowledge support from the U.S. National Science Foundation under Award No. DMR-1207293.

[1]T. S. Böscke, J. Müller, D. Bräuhaus, U. Schröder, and U. Böttger, Appl. Phys. Lett. **99**, 102903 (2011).
[2]J. Müller, U. Schröder, T. S. Böscke, I. Müller, U. Böttger, L. Wilde, J. Sundqvist, M. Lemberger, P. Kuücher, T. Mikolajick, and L. Frey, J. Appl. Phys. **110**, 114113 (2011).
[3]S. Mueller, J. Mueller, A. Singh, S. Riedel, J. Sundqvist, U. Schroeder, and T. Mikolajick, Adv. Funct. Mater. **22**, 2412 (2012).
[4]J. Müller, T. S. Böscke, U. Schröder, S. Mueller, D. Bräuhaus, U. Böttger, L. Frey, and T. Mikolajick, Nano Lett. **12**, 4318 (2012).
[5]S. Mueller, C. Adelmann, A. Singh, S. Van Elshocht, U. Schroeder, and T. Mikolajick, ECS J. Solid State Sci. Technol. **1**, N123 (2012).
[6]T. Schenk, S. Mueller, U. Schroeder, R. Materlik, A. Kersch, M. Popovici, C. Adelmann, S. Van Elshocht, and T. Mikolajick, in *2013 Proceedings of European Solid-State Device Research Conference* (IEEE, 2013), pp. 260–263.
[7]M. Hyuk Park, H. Joon Kim, Y. Jin Kim, W. Lee, T. Moon, and C. Seong Hwang, Appl. Phys. Lett. **102**, 242905 (2013).
[8]T. Shimizu, T. Yokouchi, T. Shiraishi, T. Oikawa, P. S. S. R. Krishnan, and H. Funakubo, Jpn. J. Appl. Phys., Part **53**, 09PA04 (2014).
[9]C. Cheng and A. Chin, IEEE Electron Device Lett. **35**, 138 (2014).
[10]S. Mueller, J. Müller, R. Hoffmann, E. Yurchuk, T. Schlösser, R. Boschke, J. Paul, M. Goldbach, T. Herrmann, A. Zaka, U. Schröder, and T. Mikolajick, IEEE Trans. Electron Devices **60**, 4199 (2013).
[11]E. Yurchuk, J. Müller, J. Paul, T. Schlösser, D. Martin, R. Hoffmann, S. Müeller, S. Slesazeck, U. Schröeder, R. Boschke, R. van Bentum, and T. Mikolajick, IEEE Trans. Electron Devices **61**, 3699 (2014).
[12]M. H. Park, H. J. Kim, Y. J. Kim, T. Moon, K. Do Kim, and C. S. Hwang, Adv. Energy Mater. **4**, 1400610 (2014).
[13]S. Mueller, J. Müller, U. Schroeder, and T. Mikolajick, IEEE Trans. Device Mater. Reliab. **13**, 93 (2013).
[14]P. D. Lomenzo, P. Zhao, Q. Takmeel, S. Moghaddam, T. Nishida, M. Nelson, C. M. Fancher, E. D. Grimley, X. Sang, J. M. LeBeau, and J. L. Jones, J. Vac. Sci. Technol., B **32**, 03D123 (2014).
[15]E. Yurchuk, J. Müller, S. Knebel, J. Sundqvist, A. P. Graham, T. Melde, U. Schröder, and T. Mikolajick, Thin Solid Films **533**, 88 (2013).
[16]P. D. Lomenzo, Q. Takmeel, C. Zhou, Y. Liu, C. M. Fancher, J. L. Jones, S. Moghaddam, and T. Nishida, Appl. Phys. Lett. **105**, 072906 (2014).
[17]D. Martin, J. Müller, T. Schenk, T. M. Arruda, A. Kumar, E. Strelcov, E. Yurchuk, S. Müller, D. Pohl, U. Schröder, S. V. Kalinin, and T. Mikolajick, Adv. Mater. **26**, 8198 (2014).
[18]D. Zhou, J. Xu, Q. Li, Y. Guan, F. Cao, X. Dong, J. Müller, T. Schenk, and U. Schröder, Appl. Phys. Lett. **103**, 192904 (2013).
[19]P. Polakowski, S. Riedel, W. Weinreich, M. Rudolf, J. Sundqvist, K. Seidel, and J. Müller, in *2014 IEEE 6th International Memory Workshop* (IEEE, 2014), pp. 1–4.
[20]T. Schenk, E. Yurchuk, S. Mueller, U. Schroeder, S. Starschich, U. Böttger, and T. Mikolajick, Appl. Phys. Rev. **1**, 041103 (2014).
[21]C. J. Brennan, Integr. Ferroelectr. **2**, 73 (1992).
[22]C. J. Brennan, MRS Proc. **243**, 141 (1991).
[23]R. R. Mehta, B. D. Silverman, and J. T. Jacobs, J. Appl. Phys. **44**, 3379 (1973).
[24]M. M. Hussain, N. Moumen, J. Barnett, J. Saulters, D. Baker, and Z. Zhang, Electrochem. Solid-State Lett. **8**, G333 (2005).
[25]S. Mueller, S. R. Summerfelt, J. Müller, U. Schroeder, and T. Mikolajick, IEEE Electron Device Lett. **33**, 1300 (2012).
[26]L. A. Giannuzzi and F. A. Stevie, Micron **30**, 197 (1999).
[27]M. Sugiyama and G. Sigesato, J. Electron Microsc. (Tokyo) **53**, 527 (2004).
[28]L. A. Giannuzzi, J. L. Drown, S. R. Brown, R. B. Irwin, and F. A. Stevie, Microsc. Res. Tech. **41**, 285 (1998).
[29]J. Mayer, L. A. Giannuzzi, T. Kamino, and J. Michael, MRS Bull. **32**, 400 (2007).
[30]S. Bals, W. Tirry, R. Geurts, Z. Yang, and D. Schryvers, Microsc. Microanal. **13**, 80 (2007).
[31]N. I. Kato, J. Electron Microsc. (Tokyo) **53**, 451 (2004).
[32]D. Zhou, J. Müller, J. Xu, S. Knebel, D. Bräuhaus, and U. Schröder, Appl. Phys. Lett. **100**, 082905 (2012).
[33]L. Pintilie, I. Boerasu, M. J. M. Gomes, T. Zhao, R. Ramesh, and M. Alexe, J. Appl. Phys. **98**, 124104 (2005).
[34]M. Kohli, P. Muralt, and N. Setter, Appl. Phys. Lett. **72**, 3217 (1998).
[35]T. D. Huan, V. Sharma, G. A. Rossetti, and R. Ramprasad, Phys. Rev. B **90**, 064111 (2014).
[36]N. Umezawa, K. Shiraishi, T. Ohno, H. Watanabe, T. Chikyow, K. Torii, K. Yamabe, K. Yamada, H. Kitajima, and T. Arikado, Appl. Phys. Lett. **86**, 143507 (2005).
[37]V. Cuny and N. Richard, J. Appl. Phys. **104**, 033709 (2008).
[38]M. H. Park, H. J. Kim, Y. J. Kim, W. Jeon, T. Moon, and C. S. Hwang, Phys. Status Solidi RRL **8**, 532 (2014).
[39]T. Schenk, U. Schroeder, M. Pešić, M. Popovici, Y. V. Pershin, and T. Mikolajick, ACS Appl. Mater. Interfaces **6**, 19744 (2014).
[40]S. Bernacki, L. Jack, Y. Kisler, S. Collins, S. D. Bernstein, R. Hallock, B. Armstrong, J. Shaw, J. Evans, B. Tuttle, B. Hammetter, S. Rogers, B. Nasby, J. Henderson, J. Benedetto, R. Moore, C. R. Pugh, and A. Fennelly, Integr. Ferroelectr. **3**, 97 (1993).
[41]A. K. Tagantsev, I. Stolichnov, N. Setter, J. S. Cross, and M. Tsukada, Phys. Rev. B **66**, 214109 (2002).
[42]T. S. Böscke, J. Müller, D. Bräuhaus, U. Schröder, and U. Böttger, in *2011 International Electron Devices Meeting* (IEEE, 2011), pp. 24.5.1–24.5.4.
[43]B. Jaffe, Proc. IRE **49**, 1264 (1961).
[44]X. Hao, J. Zhai, L. B. Kong, and Z. Xu, Prog. Mater. Sci. **63**, 1 (2014).
[45]S. S. N. Bharadwaja and S. B. Krupanidhi, J. Appl. Phys. **89**, 4541 (2001).